JACS
JOURNAL OF THE AMERICAN CHEMICAL SOCIETY
Article
pubs.acs.org/JACS

# Design and Synthesis of New Stable Fluorenyl-Based Radicals

Yi Tian, Kazuyuki Uchida, Hiroyuki Kurata,‡ Yasukazu Hirao, Tomohiko Nishiuchi, and Takashi Kubo*

Department of Chemistry, Graduate School of Science, Osaka University, Toyonaka, Osaka 560-0043, Japan

Supporting Information

**ABSTRACT:** Organic neutral radicals have long fascinated chemists with a fundamental understanding of structure−reactivity relationships in organic reactions and with applications as new functional materials. However, the elusive nature of these radicals makes the synthesis, isolation, and characterization very challenging. In this work, the synthesis of three long-lived, fluorenyl-based radicals are reported. The geometry and electronic structures of these radicals were systematically investigated with a combination of various experimental methods, besides density functional theory (DFT) calculations, which include X-ray crystallographic analysis, electron spin resonance (ESR), electron nuclear double resonance (ENDOR), cyclic voltammetry, and UV−vis−NIR measurements. Their half-life periods ($\tau_{1/2}$) in air-saturated solution under ambient conditions were also determined. Surprisingly, all three radicals showed remarkable stabilities: $\tau_{1/2}$ = 7, 3.5, and 43 days.

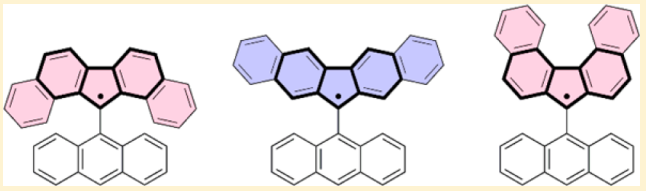

## INTRODUCTION

In recent years, interest has grown for the development of stable organic radicals as new functional molecular materials, because their open-shell electronic structures show unique technologically relevant properties.[1−3] By virtue of having external stimuli (such as light, and electric and magnetic fields)-responsive spin structures, stable organic radicals provide novel schemes for performing spin memory and logic operations, and open avenues for quantum information science and quantum computers.[4,5] The multistage redox ability induced by small energy gaps between frontier orbitals of some organic radicals or radical polymers is crucial for their application as electrode-active materials in next-generation batteries, which feature fast electrode kinetics, reactant recyclability, and high redox capacity.[6−8] The good redox properties of organic radicals are also important in the preparation of responsive bistable molecular materials with magnetic and/or conducting properties.[9,10] Further, because the large Boltzmann polarization of unpaired electrons in organic radicals can be transferred to proximal nuclei via microwave electron−nuclear transitions, they are currently arousing a great interest in the promising dynamic nuclear polarization (DNP) technique, which can increase the NMR signal intensities of solids and liquids by 2 to 3 orders of magnitude.[11−13] In addition, the usage of stable organic radicals as reporter molecules to obtain structural, dynamic, and reactivity information on other systems in electron spin resonance (ESR) spectroscopy by techniques such as spin labeling, spin trapping, and ESR imaging are well-known,[2] and because radicals show a characteristic and narrow band in the oxygen-sensitive ESR spectrum, they can be used as chemical sensors of oxygen and reactive oxygen species in chemical and biological systems.[14,15] Radicals also have been exploited in catalysis, polymerization processes, and antioxidants.[2,16−18] Attaching persistent organic radicals to inorganic surfaces to explore their novel properties and applications in those hybrid materials has been studied.[19] Recently, stable organic radicals were even used as a stabilizer for pentacene derivatives,[20] and a method to manipulate the stability of radicals by an external controller (pH in this case) was also introduced for future applications.[21]

The synthesis of radicals with sufficient stabilities is the precondition for their further applications in materials science. In most cases, kinetic stabilization by protecting the spin center with steric hindrance and thermodynamic stabilizations by spin delocalization are both essential for the stabilities of radicals. Unlike heteroatom-centered radicals, which are well studied in terms of the functionality,[22] hydrocarbon radicals have been far from application because of a strong propensity for $\sigma$-dimerization originating from the strength of the carbon−carbon bond.[23] Because physical properties of hydrocarbon radicals depend predominantly on the topology of the $\pi$-electron array, the development of new hydrocarbon radicals is key to new basic molecular skeletons that promise novel and diverse applications of spin materials. Furthermore, studying structure−property relationships will provide valuable information for the molecular design.

The cyclopentadienyl (Cp) radical species is one of the simplest members of conjugated hydrocarbon radicals, but further property investigation and application have been hampered by the inherent high reactivity.[24] By far, only a few of them have been isolated in crystalline form, and those radicals are stabilized by steric effect, hyperconjugative stabilization, or spin delocalization (Chart 1).[24−26] More effective way to delocalize an unpaired electron is annulating the $\pi$-system to the cyclopentadienyl center. Benzannulation of a cyclopentadienyl center forms a fluorenyl structure, which is widely used as a building block in organic molecules for

Received: July 17, 2014
Published: August 18, 2014

   dx.doi.org/10.1021/ja507005c | J. Am. Chem. Soc. 2014, 136, 12784−12793

**Chart 1. Cyclopentadienyl and Fluorenyl Radicals Isolated So Far in Crystalline Form**

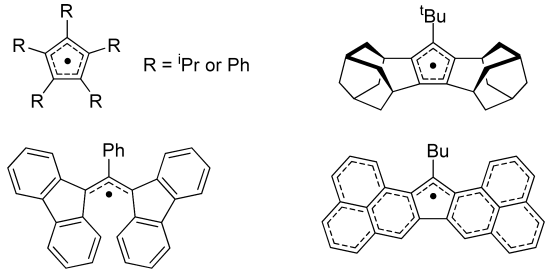


material usage because of the high fluorescence quantum yield, hole-transporting property, high electron affinity, etc. Haley, Tobe, and many other research groups did tremendous work in this field.[27−33] However, although it provides $\pi$-delocalization to the Cp radical center, the fluorenyl radical itself is still a transient species with a large spin coefficient (0.61) at the center position.[34−37] Fluorenyl-based radicals can only be isolated when large steric hindrances exist[38,39] or when the spin is more highly delocalized by two larger annulated $\pi$-systems.[40]

On the other hand, the 9-anthryl group has a stabilization effect for some radical centers, such as the newly reported fluorenyl monoradical (Chart 2). This radical was so long-lived

**Chart 2. Wu's Fluorenyl Radicals Stabilized by 9-Anthryl Groups**

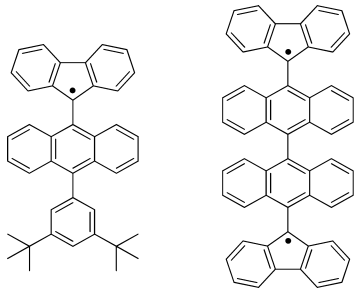

as to be purified by column chromatography and be observed by conventional UV−vis and ESR measurements. Moreover, the stable tetrabenzo-Chichibabin's hydrocarbon derivative can also be considered as an open-shell biradical that is stabilized kinetically by two 9-anthryl groups.[41a] Recent progress in the development of stable biradicals have opened the way for applying weakly coupled electrons to nonlinear optics, stimuli-responsive magnetic activity, etc.[41b] Whether the 9-anthryl group can be used as a general stabilization group for other kinds of radicals is of great importance for neutral radical research.

Inspired by those studies, our strategy toward thermodynamic stabilization of fluorenyl-based radicals is by $\pi$-extension of the fluorenyl unit with two aromatic benzene rings, and on the basis of the position of the extended benzene rings, we designed three types of target radicals, which can be called a-type, b-type, and c-type (Chart 3). Kinetic stabilization was achieved by applying the steric hindrance of the 9-anthryl group to the center position of fluorenyl. Such a design can possibly also improve the solubility due to the orthogonal conformation of the anthryl with respect to the dibenzofluorenyl moieties.

In this article, we demonstrate detailed research on the synthesis of those fluorenyl-based radicals. The electronic and

**Chart 3. Three Types of Target Fluorenyl-Based Radicals**

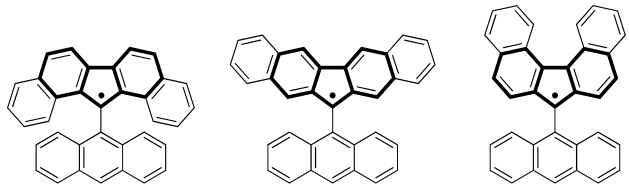


geometric structures were systematically studied by X-ray crystallography, electron spin resonance (ESR), electron nuclear double resonance (ENDOR), cyclic voltammetry, and UV−vis−NIR absorption and assisted by density functional theory (DFT) calculations. Their stabilities in solution under ambient conditions and decomposed species were also investigated carefully. We find that different benzannulations greatly influence the properties (reactive position, stabilities, decomposition products, etc.) of radicals, because each benzannulation position leads to different spin distribution and also a difference in steric hindrance toward the spin center.

## RESULTS AND DISCUSSION

**Syntheses.** The stepwise synthetic procedure for target radicals is outlined in Scheme 1. Three types of ketone intermediates were synthesized from commercially available starting materials and according to literature with some modifications of a few steps. **6** was oxidized by triton-B in pyridine to give **3a** as a crude product as reported in previous procedures.[40,42] **3b** was obtained by repeating the tandem Diels−Alder aromatization reaction.[43,44] **12** reacted with acetic anhydride at reflux for 1 h and followed by heating at 300 °C for 3 h to give **3c** in moderate yield.[45,46] The ketone intermediates were treated with lithiated anthracene to give three types of alcohol precursors in high yields, which were reduced with triethylsilane to give the hydrocarbon precursors. All of the intermediates were well characterized by $^{1}$H and $^{13}$C NMR and mass spectroscopy. In the first method we tried to synthesize the radicals by oxidation. **1b** can be obtained as brown crystals by oxidizing with DDQ in toluene in a sealed tube under vacuum, but the a-type hydrocarbon precursor only induced decomposition in this method even when using the weaker oxidant chloranil. Because **1b** showed very high stability, which indicates that the radicals may survive long enough to be purified by column chromatography, the reduction method was tried and it succeeded in the preparation of **1a** and **1c** with $SnCl_2$.

**X-ray Crystallographic Analyses.** Single crystals suitable for X-ray crystallographic analysis were successfully grown by recrystallization from various solvents (toluene, dichloromethane, ethyl acetate, *N*,*N*-dimethylformamide (DMF), or *n*-hexane) under argon flow, and crystal structures of **1a−c** determined at 200 K are shown in Figure 1. **1a** dimerized in a position on the dibenzofluorenyl moiety to give a $\sigma$-dimer (**1a**$_2$) in the crystalline state. The length of the $\sigma$-bond connecting two **1a** is 1.597(4) Å, and such a long bond length indicates that it is a relatively weak bond. The twist angle between the dibenzofluorenyl and anthryl moiety in the crystal is 83° (mean value). In contrast, **1b** could be obtained as an unassociated monoradical in the crystalline state. The twist angle between the dibenzofluorenyl and the anthryl moiety is 65° (mean value). Recrystallization of **1c** from toluene, dichloromethane,


dx.doi.org/10.1021/ja507005c | J. Am. Chem. Soc. 2014, 136, 12784−12793

**Scheme 1. Synthetic Route to Radicals 1a–c**[a]

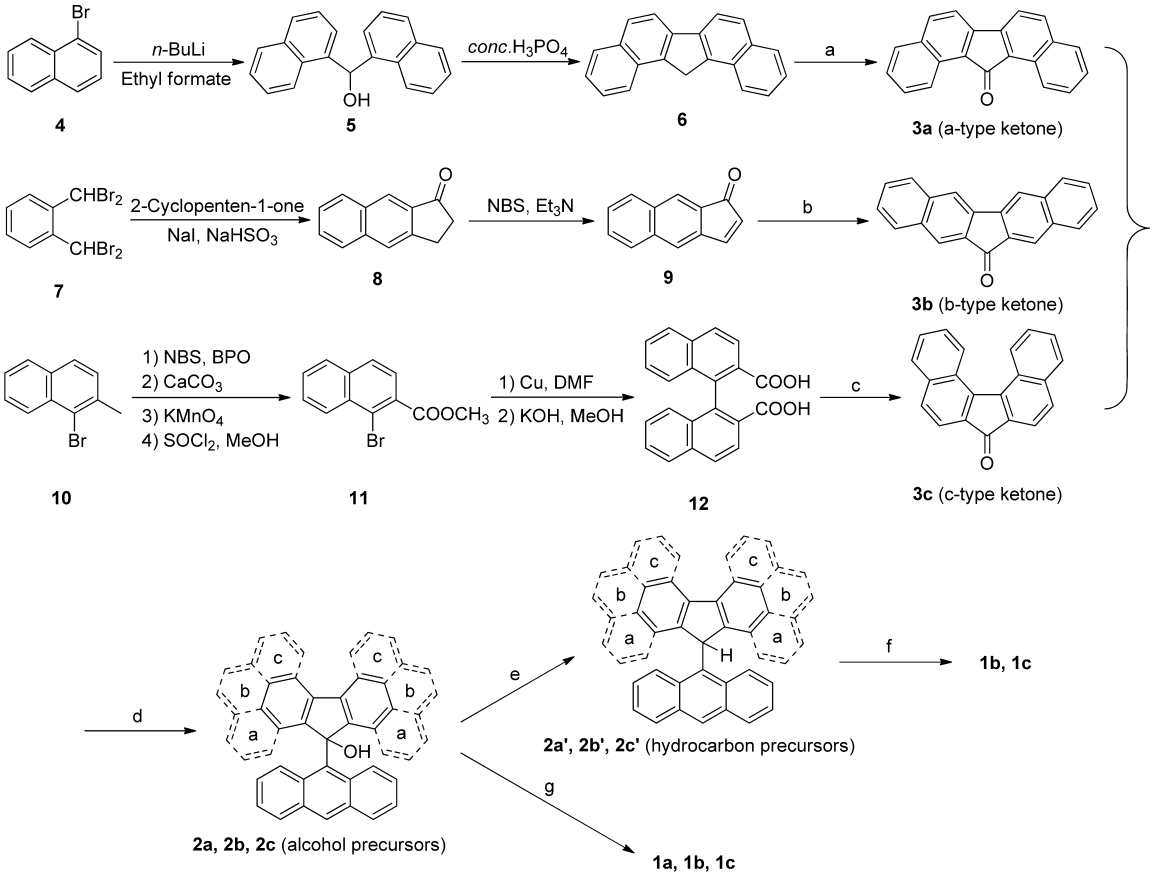


[a]Reagents and conditions: (a) triton-B, pyridine, rt, quant. (crude); (b) $\alpha,\alpha,\alpha',\alpha'$-tetrabromo-*o*-xylene (**7**), NaI, DMF, 80 °C, quant. (crude); (c) acetic anhydride, 140 to 300 °C, 37%; (d) 9-bromoanthracene, *n*-BuLi, THF, −78 °C to rt, 92% (**3a**), 92% (**3b**), 98% (**3c**); (e) $Et_3SiH$, TFA, dichloromethane, rt, 73% (**2a′**), 67% (**2b′**), 66% (**2c′**); (f) DDQ, toluene, *n*-hexane, 50 °C, 38% (**1b**), 73% (**1c**), isolated yields in a crystalline form; (g) $SnCl_2$, dichloromethane, rt, 35% (**1a**), 33% (**1b**), 82% (**1c**), isolated yields in a crystalline form.

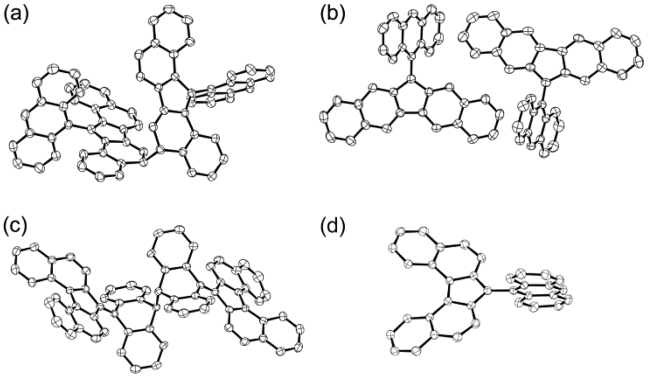


**Figure 1.** ORTEP drawings of (a) $\mathbf{1a}_2$ ($\sigma$-dimer), (b) **1b**, (c) $\mathbf{1c}_2$ ($\sigma$-dimer), and (d) **1c** with thermal ellipsoids at 50% probability. Hydrogen atoms are omitted for clarity.

ethyl acetate, or DMF solutions also gave a $\sigma$-dimer ($\mathbf{1c}_2$) in crystalline form; however, the dimerization position is not on the dibenzofluorenyl moiety but instead at the 10-position of the anthryl group. The length of this weak $\sigma$-bond is 1.576(5) Å. $\mathbf{1c}_2$ adopted a folded conformation between the dibenzofluorenyl and anthryl moieties, and the bond length between them is 1.368(5) Å, which is typical for an olefin bond. Surprisingly, recrystallization of **1c** from a *n*-hexane solution gave unassociated monoradical in the crystalline state. The twist angle between the dibenzofluorenyl and anthryl moieties in the crystal is 60°. The twist angle of **1c** is smaller than that of **1b**, which is presumably due to a crystal packing force, because UB3LYP/6-31G** calculations show small differences in the twist angles: 68° and 66° for **1b** and **1c**, respectively.

**ESR, ENDOR, VT-ESR, and $^1$H NMR Measurements.** The X-band ESR spectra of those three radicals were measured in oxygen-free toluene at 240 K, and well-resolved multiline spectra were obtained ($g$ = 2.003), which is the unambiguous evidence of the existence of those radicals in solution state. The proton hyperfine coupling constants ($a_H$) of **1b** can be determined by computer simulation. However, the ESR spectra of **1a** and **1c** cannot be simulated because of the very complex pattern; therefore, we performed the ENDOR technique for the most reliable $a_H$ values. Figure 2 shows the observed and simulated ESR spectra of **1a**, **1b**, and **1c** along with the $a_H$ values (the $^1$H ENDOR spectra are shown in Figures S1 and S2, Supporting Information). As shown in Figure 2, the agreement between the experimental and theoretical $a_H$ values indicate that the spin distribution structures of the radical molecules are in well correspondence with the calculated spin density maps. **1a** shows three major lines in the hyperfine pattern due to the large population of unpaired electron at C9 ($a_H$ = 0.418, for atom numbering in dibenzofluorenyl cores, see Figure 4). **1b** also gives three major lines because of the large spin density at C3 ($a_H$ = 0.533), but its hyperfine pattern is


dx.doi.org/10.1021/ja507005c | J. Am. Chem. Soc. 2014, 136, 12784–12793

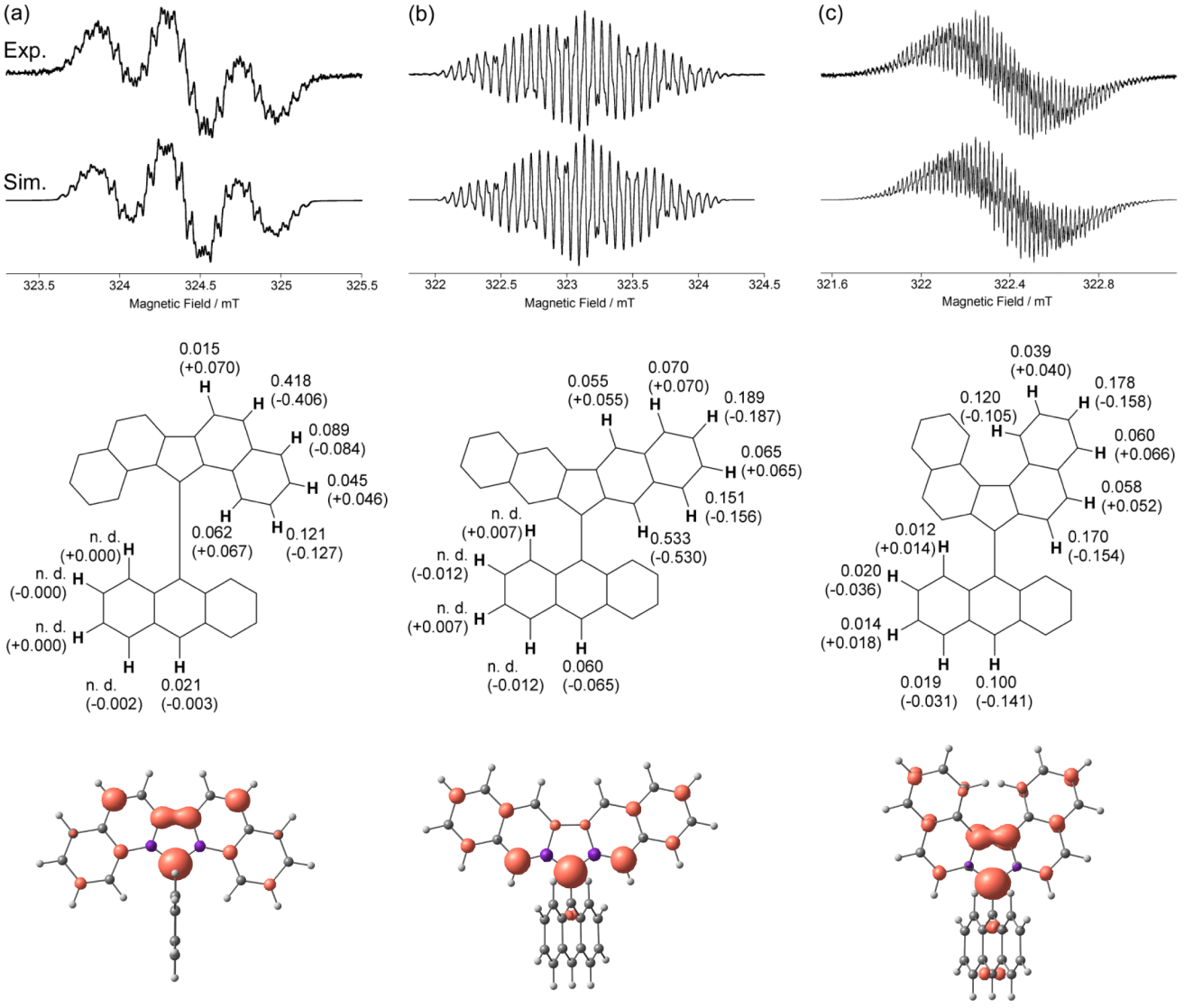


**Figure 2.** (Top) Observed ($1 \times 10^{-4}$ M in toluene, at 240 K, $g = 2.003$) and simulated ESR spectra of (a) **1a**, (b) **1b**, and (c) **1c**. (Middle) Hyperfine coupling constants ($a_H$) determined. In parentheses, $a_H$ values estimated with a UBLYP/6-31G**//UB3LYP/6-31G** method and the McConnell model ($Q = -2.4$ mT). (Bottom) Spin density maps calculated with the same calculation method. Red and purple surfaces represent $\alpha$ and $\beta$ spin densities drawn at 0.004 e/au$^3$ level, respectively.

significantly influenced by relatively large spin density on other positions of the dibenzofluorenyl moiety. For example, the second and third large spin density positions with $\alpha$ protons in **1b** are C5 ($a_H = 0.151$) and C7 ($a_H = 0.189$), but in **1a** they are C5 ($a_H = 0.121$) and C7 ($a_H = 0.089$). **1c** exhibits only one main line because the large spin density positions lack protons. In addition, the anthryl group of **1c** possesses spin density larger than that of **1a** and **1b**.

The intensities of the ESR signals of **1a**–**c** showed different behaviors in the variable-temperature (VT) ESR measurement (Figure 3). The ESR signal intensity of **1a** drastically decreased upon cooling because of the $\sigma$-dimerization. The linear dependence of ln $K_D$ (dimerization constant) afforded the thermodynamic parameters $\Delta H_D = -32$ kJ mol$^{-1}$ and $\Delta S_D = -63$ J K$^{-1}$ mol$^{-1}$ (Figure 3) for the $\sigma$-dimerization. It is noted that **1a** almost dissociates into monomeric species in a dilute solution state at room temperature. In contrast, the ESR signal intensity of **1b** almost remained unchanged even at 180 K, and that of **1c** only showed a tiny amount of decrease at 180 K.

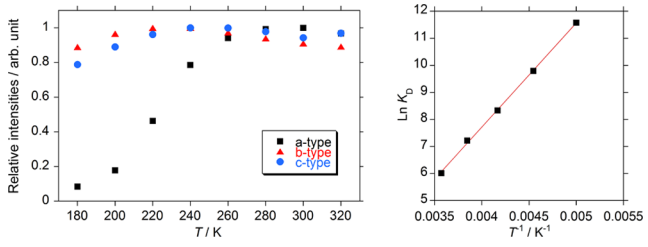


**Figure 3.** (Left) Temperature dependence of ESR signal intensities for **1a** (black square), **1b** (red triangle), and **1c** (blue circle). (Right) Temperature dependence of the dimerization constant $K_D$ of **1a**.

High tolerance of **1b** and **1c** to dimerization would come from steric protection of reactive sites by the anthryl group.

$^1$H NMR measurements, which disclosed the dissociation of $\mathbf{1c}_2$, showed a time-dependent property (Figure S3, SI). The spectrum of $\mathbf{1c}_2$ can be clearly observed at the beginning of dissolution, and then the signals disappeared after several hours. In contrast, no signal could be detected after the dissolution of


dx.doi.org/10.1021/ja507005c | J. Am. Chem. Soc. 2014, 136, 12784–12793

$1a_2$ in $CDCl_3$, because the dissociation proceeded immediately after dissolution of the crystal.

**Theoretical Calculations.** Unrestricted DFT calculations were conducted to estimate the spin distribution of **1a−c**. The spin density map calculated with a UBLYP/6-31G**//UB3LYP/6-31G** method is shown in Figure 2 (bottom). Benzannulation of the fluorenyl makes the spin delocalized on the whole dibenzofluorenyl moiety although most spin still concentrates on the fluorenyl center. The spin density on the Cp has obvious decrease compared with the nonannulated fluorenyl radical (Figure S4, SI).

One of the major spin distribution positions of **1a** is C9, and the lack of steric protection makes the dimerization in the crystallization progress very reasonable. The main spin distribution position in **1b** is in the very steric C3, which makes the intermolecular dimerization difficult. In radical **1c**, although the main spin distribution positions on the dibenzofluorenyl moiety are well protected by the anthryl group and the annulated benzene ring, some spin distributed on the 10-position of the anthryl group makes dimerization proceed at this spot when forming crystals.[47]

For deeper understanding of the electronic structure of dibenzofluorenyls, bond lengths and nucleus-independent chemical shift (NICS)[48] values of the parent dibenzofluorenyls (**1a′−c′**) were also calculated (Figure 4) at the level of

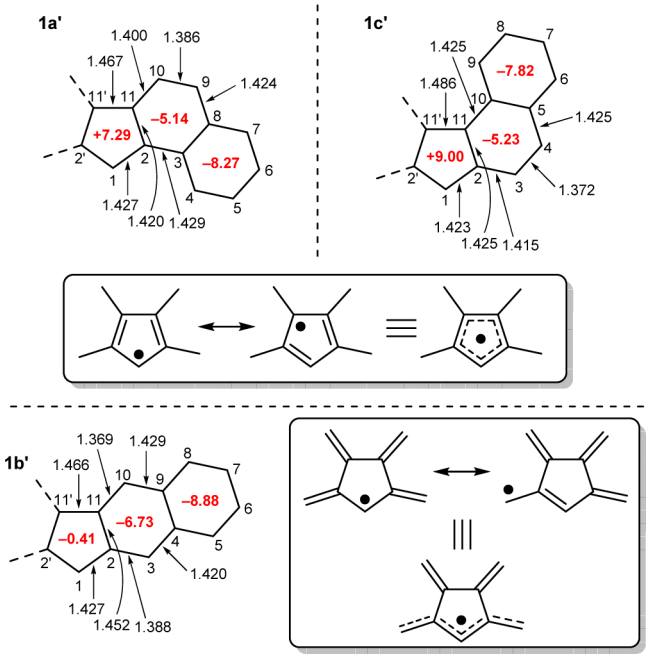


**Figure 4.** Bond lengths and NICS(1) values (in red) of the parent dibenzofluorenyls (**1a′**, **1b′**, and **1c′**) calculated with UB3LYP/6-31G** and GIAO-UB3LYP/6-311+G**//UB3LYP/6-31G** methods, respectively. At the same level of calculation, NICS(1) of benzene is −10.19 ppm.

UB3LYP/6-31G** and GIAO-UB3LYP/6-311+G**//UB3LYP/6-31G** calculations, respectively. The theoretical bond lengths of **1b′** and **1c′** approximately correspond with observed values for **1b** and **1c**, respectively, being undoubted proof of the accuracy of our calculations. In the center Cp rings, the C1−C2 bond lengths are nearly identical for all the parent radicals (**1a′**, 1.427 Å; **1b′**, 1.427 Å; **1c′**, 1.423 Å), whereas a large difference in length is observed for the C2−C11 bonds between **1a′** (1.420 Å)/**1c′** (1.425 Å) and **1b′** (1.452 Å). In a similar way, exo bonds of the Cp ring of **1a′** (1.400, 1.429 Å)/**1c′** (1.425, 1.415 Å) are longer than that of **1b′** (1.369, 1.388 Å). These differences arise from a difference in the fusion mode of the naphthalene rings to the Cp rings. It is well-known that naphthalene possesses larger double bond character at the 1,2-bond than at the 2,3-bond. Therefore, Cp ring annulation to the 1,2 or 2,3 region of naphthalene leads to endo- or exo-double bonds at the Cp ring, respectively. Thus, the unpaired electron can enjoy cyclic delocalization in the Cp rings for **1a′**/**1c′** but not for **1b′**. Conjugation style of the Cp rings is best described as cyclopentadienyl in **1a′**/**1c′** and radialene in **1b′** (Figure 4). This idea is supported by the NICS calculation. NICS(1) values on the Cp rings of **1a′**/**1c′** are positively large, which is in accordance with the positive NICS(1) value (+13.02 ppm) of the cyclopentadienyl radical. On the other hand, the NICS(1) value of **1b′** is nearly zero, together with more aromaticity of the benzene ring beside the Cp ring, indicating no or very small contribution of cyclic conjugation in the Cp ring of **1b′**.

From the spin density and NICS calculations, an unpaired electron mainly delocalizes in fluorenyl moieties, as highlighted in red in Figure 5, and the most outer rings could benefit from aromaticity, suggesting that the stabilities of **1a−c** can actually be enhanced by benzannulation. As shown in the resonance structures, spin delocalization of a simple fluorenyl radical destructs one aromatic sextet (NICS(1) = −5.69 ppm on six-membered rings) but requires no destruction of the aromatic sextet in the dibenzofluorenyl radicals.

Next, we will focus on the association behavior of **1c**. As mentioned above, **1c** dimerizes at the 10-position of the anthryl substituent group with a drastic conformation change. We were able to locate the transition structure (**1c***) for the most-stable twisted form ⇄ a metastable folded form, by means of the quadratic synchronous transit (QST2) method at the UPM3 level of calculation and optimized at UB3LYP/6-31G** level. The structure of **1c*** is close to the folded form except that the anthryl group is contorted. The calculated enthalpy of activation ($\Delta H^{\ddagger}$) for the twisted form to **1c*** was 95.5 kJ $mol^{-1}$ (Figure 6). Although $\mathbf{1c}_2$ is more stable than the twisted form, the energy difference is just 0.6 kJ $mol^{-1}$. All these theoretical results are in line with experimental observations for **1c**. Calculations for **1b**, which gave only a monomeric radical in the solid state, also gave similar results: $\Delta H^{\ddagger}$ = 96.6 kJ $mol^{-1}$, and the σ-dimer $\mathbf{1b}_2$ is more stable than the twisted **1b** by 3.1 kJ $mol^{-1}$ (Figure S5, SI). Indeed, VT ESR experiments show only small differences in association behaviors in the solution state between **1b** and **1c**. Although the different behaviors in the solid state might be attributable to low crystallinity of $\mathbf{1b}_2$, the interplay between steric strain and conjugation would also play an important role, like that of overcrowded aromatic enes (OAEs).[49] Slight differences in the interplay might lead to different behaviors between **1b** and **1c** in the solid state. Indeed, oxygen attack occurs in a different manner between **1b** and **1c**, as shown below.

**Electrochemical Properties.** Cyclic voltammetry was performed to investigate the redox behaviors of **1a**, **1b**, and **1c** (Figure 7). Excellent electrochemical amphotericity was observed for those three radicals. The half-wave potential of the reversible oxidative waves ($E_{ox}^{1/2}$) are +0.37 V, +0.13 V, and +0.29 V for **1a**, **1b**, and **1c**, respectively, and their half-wave potentials of the reversible reductive processes ($E_{red}^{1/2}$) are −0.90 V, −1.23 V, and −0.82 V (all values vs $Fc^+$/Fc),


dx.doi.org/10.1021/ja507005c | J. Am. Chem. Soc. 2014, 136, 12784−12793

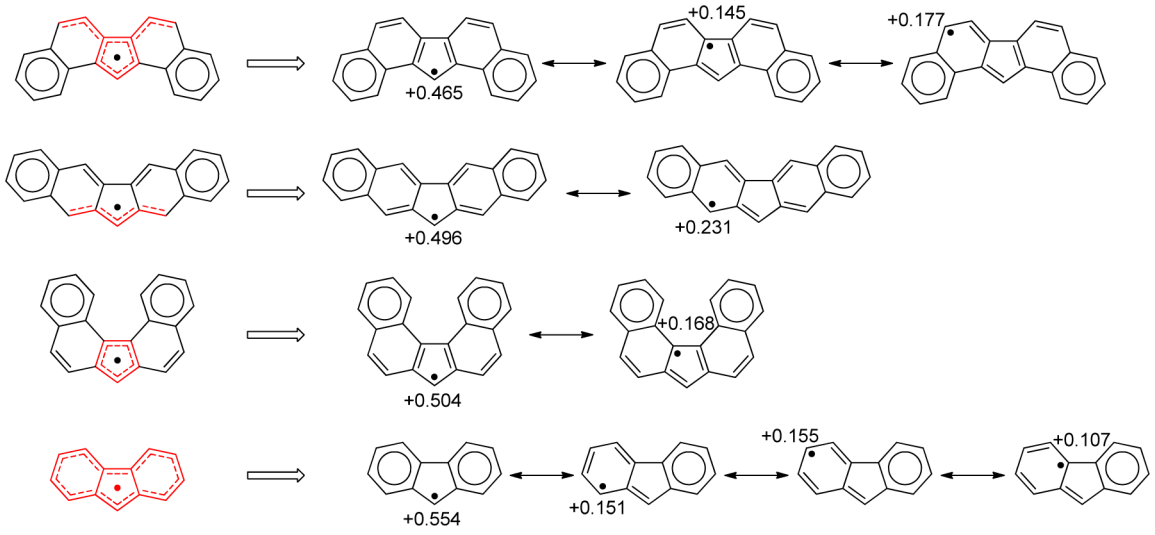


**Figure 5.** Major resonance contributors of dibenzofluorenyl radicals (**1a**′, **1b**′, and **1c**′) and fluorenyl radical. Resonance contributors with spin density of less than 0.1 are not shown. Numerals are spin densities calculated with UBLYP/6-31G**.

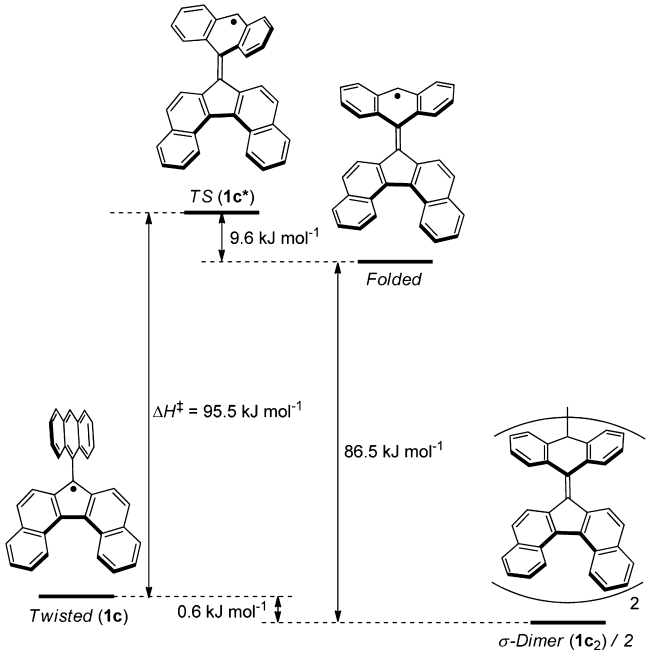


**Figure 6.** Energy diagram for twisted **1c** to $\mathbf{1c}_2$ ($\sigma$-dimer) calculated with the UB3LYP/6-31G** method.

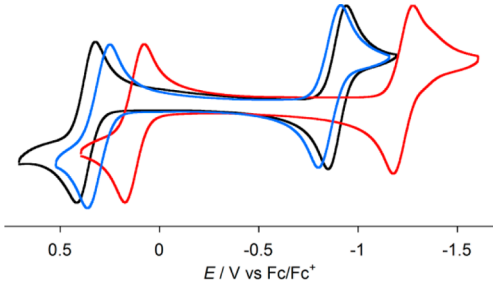


**Figure 7.** Cyclic voltammograms (V vs $Fc/Fc^+$, in 0.1 M $^nBu_4NClO_4$/dichloromethane, scan rate 100 mV/s, room temperature) of **1a** (black), **1b** (red), and **1c** (blue).

respectively. The redox waves of **1a** and **1c** show positive shift in potential with respect to those of **1b**. This shift comes from the difference in conjugation style in the Cp rings. Due to the cyclic conjugation in the Cp rings of **1a** and **1c**, both radicals experience antiaromaticity and aromaticity on the Cp rings in cation and anion state, respectively, and therefore are more difficult to oxidize and more easily reduced.

The dissociation of $\mathbf{1c}_2$ also showed a time-dependent property in CV measurement. After the crystal dissolved in dichloromethane solvent, it took 5−6 h for $\mathbf{1c}_2$ to totally dissociate into monoradical **1c** (Figure S6, SI). In contrast, $\mathbf{1a}_2$ immediately dissociated into monomeric **1a** right after the crystal dissolution.

**Optical Properties.** The UV−vis−NIR spectra of the radicals were measured in dichloromethane (Figure 8). Time-

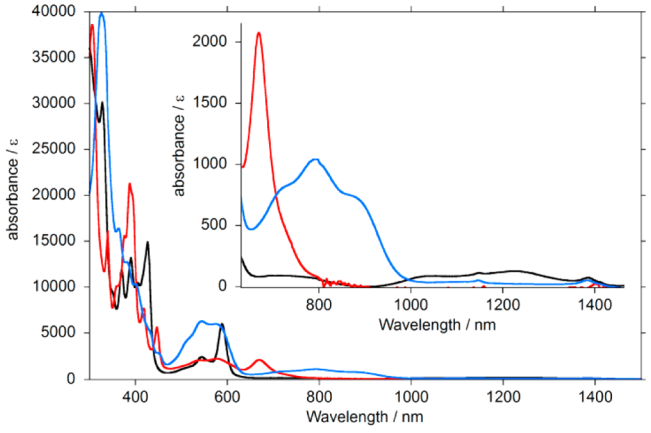


**Figure 8.** UV−vis−NIR spectra ($1.0 \times 10^{-4}$ M in dichloromethane, room temperature) of **1a** (black), **1b** (red), and **1c** (blue). Inset shows a magnified view in the NIR region.

dependent (TD) UB3LYP/6-31G** calculation well explained those spectra (Supporting Information). **1a** displayed a very weak absorption band with the maximum at 1220 nm ($\varepsilon$ ~100), which is induced by the transition from the next HOMO (NHOMO) $\beta$-spin (115B) to SOMO $\beta$-spin (116B), and a sharp absorption band with the maximum at 588 nm ($\varepsilon$ 6000), along with a shoulder at 544 nm ($\varepsilon$ 2300), belongs to the fourth HOMO $\beta$-spin (113B) to 116B and the fifth HOMO


dx.doi.org/10.1021/ja507005c | J. Am. Chem. Soc. 2014, 136, 12784−12793

$\beta$-spin (112B) to 116B, respectively. In those transitions, electrons were excited from periphery naphthalene delocalized orbitals (115B, 113B, and 112B) to the center Cp ring delocalized orbital (116B), affording cyclopentadienyl anion conjugation in the excited states. Also for **1c**, a very low-energy transition from the NHOMO $\beta$-spin (115B) to SOMO $\beta$-spin (116B) was predicted to be observed at 1277 nm by the TD calculation. Unfortunately, the lowest-energy band could not be detected because of the low intensity. The next lowest-energy band was observed as a broad absorption around 794 nm ($\varepsilon$ 1000), which was assigned to the excitation from second HOMO $\beta$-spin (114B) to SOMO $\beta$-spin (116B), and another two absorption bands appearing with absorption maxima at 574 nm ($\varepsilon$ 6000) and 544 nm ($\varepsilon$ 6300) were because of the excitation from the second HOMO $\beta$-spin (114B) to LUMO $\beta$-spin (117B) and fourth HOMO $\beta$-spin (112B) to SOMO $\beta$-spin (116B), respectively. Those excitations in **1c** were also the process that results in spin transfer to the center Cp ring.

The difference in dissociation progress from $\sigma$-dimer to monoradical in solutions of **1a** and **1c** was also observed in UV−vis−NIR measurements (Figure S7, SI). Dissolution of $\mathbf{1a}_2$ in dichloromethane instantly afforded a spectrum of monomeric **1a**, whereas $\mathbf{1c}_2$ took a long time to completely dissociate into the monomeric state.

In contrast to **1a** and **1c**, **1b** showed a lowest-energy absorption band in the visible region. The first absorption band around 669 nm ($\varepsilon$ 2100) is mainly contributed by the transition from NHOMO $\beta$-spin (115B) to SOMO $\beta$-spin (116B), which is an intramolecular charge transfer band from anthryl group to dibenzofluorenyl. The band starting at 577 nm ($\varepsilon$ 2200) with vibronic progression is assignable to the transition from third HOMO $\beta$-spin (114B) to SOMO $\beta$-spin (116B). This band would also include the transition from SOMO $\alpha$-spin (116A) to second LUMO $\alpha$-spin (118A). It is notable that the excitation behavior of **1b** is different from that of **1a** and **1c**, like electrochemical behaviors.

**Mechanochemical Properties.** The $\sigma$-dimers $\mathbf{1a}_2$ and $\mathbf{1c}_2$ showed mechanochromic properties in solid-state UV−vis−NIR measurements (Figures S8 and S9, SI), in which well ground crystals of $\mathbf{1a}_2$ and $\mathbf{1c}_2$ induced drastic spectral changes. Red crystals of $\mathbf{1a}_2$ turned to green-brown powder when grinding, and $\mathbf{1c}_2$ became purple powder from orange crystals (Figure 9). The brown and purple colors correspond with the colors of monomeric radicals **1a** and **1c**, respectively. This indicates that the dissociation from $\sigma$-dimer to monoradical can be a mechanochemical process.[50]

**Stabilities and Decompositions.** The stabilities of **1a−c** in toluene in air at room temperature under dark conditions were measured by ESR, and all three radicals showed significant stabilities. The half-lifetime ($\tau_{1/2}$) refers to the period of time to decrease the normalized ESR intensity by half. The $\tau_{1/2}$ of **1a** and **1b** turned out to be 7 and 3.5 days, respectively. **1c** showed the highest stability with $\tau_{1/2}$ of 43 days. The decomposition progress is in approximate correspondence with the first-order kinetic equations (Figures S10−S12, SI). The long lifetimes of **1a−c** rely on kinetic stabilization of the 9-anthryl group as well as thermodynamic stabilization by spin delocalization. The bulky and rigid skeleton of anthracene effectively protects spin centers from the attack of small molecules such as oxygen and solvents and also from self-association.

Although the decomposition of each radical in an air-saturated solution gave several products, many of them were in amounts too small to be separated and identified. However, the major decomposed products were determined successfully. Hydrogen abstraction from solvents or moisture is a main decomposition pathway for the three radicals, which are the hydrocarbon precursors **2a′**, **2b′**, and **2c′** as products. Oxidation with oxygen was another major decomposition reaction for **1b** and **1c**. **1b** was oxidized at the fluorenyl moiety to give a ketone compound, whereas oxidation occurred at the 10-position of the anthryl group of **1c** (Chart 4). The structural identifications were performed using detailed analysis of $^1$H and $^{13}$C NMR spectra including two-dimensional NMR spectroscopy (COSY, NOESY, HMQC, and HMBC; see Supporting Information). **1a** gave the most complex decomposed products, except for the hydrogen abstraction product. Some low solubility and inseparable compounds (green colored, tailing on TLC) were observed in very small amounts and also a totally insoluble greenish black residue in some amount, possibly because the unprotected spin centers on the fluorenyl moiety led to some complicated electron transfer or disproportionation reactions.[2] **1b** also gave small amounts of other decomposed products besides the identified hydrogen abstraction and oxidation compounds. **1c** showed the highest reaction specificity, and only two to three other kinds of decomposed products were observed in trace amounts.

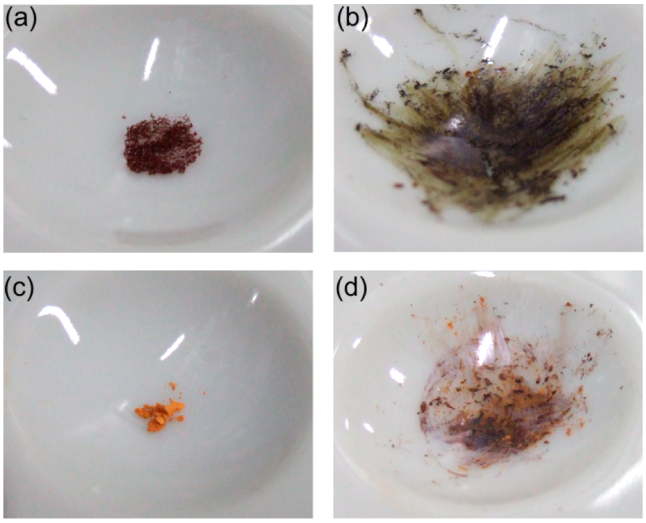


**Figure 9.** Mechanochromic behavior of $\mathbf{1a}_2$ and $\mathbf{1c}_2$. (a) Before and (b) after grinding powder of $\mathbf{1a}_2$. (c) Before and (d) after grinding powder of $\mathbf{1c}_2$.

**Chart 4. Oxidized Products of 1b and 1c**

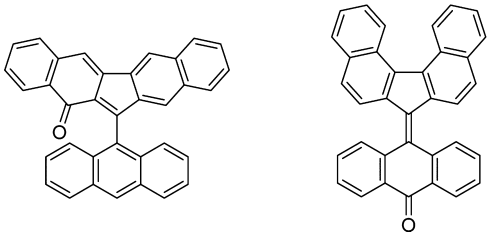

## CONCLUSION

In summary, three fluorenyl-based radical isomers (**1a−c**) were prepared. The attachment of the 9-anthryl group at the most reactive site of the fluorenyl moiety efficiently stabilizes the radicals kinetically, and benzannulation of the fluorenyl center


dx.doi.org/10.1021/ja507005c | J. Am. Chem. Soc. 2014, 136, 12784−12793

increases the stability of the radicals thermodynamically. Their electronic properties were systematically investigated by several experimental methods and assisted by DFT calculations. All three radicals showed significant stabilities; the half-lives of **1a**, **1b**, and **1c** in air-saturated toluene under ambient conditions were 7, 3.5, and 43 days, respectively. **1b** could be isolated as an unassociated monoradical in crystalline form, whereas **1a** gave $\sigma$-dimers in crystal state. **1c** existed in solid state in both unassociated monoradical and $\sigma$-dimer forms. The spin structures of those radicals were unambiguously determined by solution ESR and ENDOR measurements along with theoretical calculations. The ESR signals of **1a** were intensively decreased at low temperature, indicating that dimerization in solution proceeded. In contrast, **1b** and **1c** did not show obvious signal decrease in VT ESR measurements. Three radicals showed amphoteric redox properties in CV measurements. **1c** needed 5−6 h to finish dissociation of the $\sigma$-dimer after dissolution whereas **1a** could dissociate immediately. UV and $^1$H NMR spectra also revealed this phenomenon. Solid UV measurements disclosed mechanochromic properties of crystals of $\mathbf{1a}_2$ and $\mathbf{1c}_2$ ($\sigma$-dimers).

A different manner of benzannulation to fluorenyl radical leads to a variety of structures and properties in solution and solid states. Although these varied behaviors are ascribed to the difference in the conjugation style of spin delocalization (that is, cyclic for **1a** and **1c**, and linear for **1b**), anthracene as a substituent would also play an important role. The bulky and rigid skeleton of anthracene effectively protects a spin center with large spin density (∼0.5) from $\sigma$-dimerization and oxygen attack, and at the same time, the high ability of anthracene to pull an attached spin into its meso-position results in drastic conformation change from twisted to folded forms. Our results suggest that combination of spin-localized radicals and anthracene is a strategy for molecular design that opens new avenues for spin-based materials.

## EXPERIMENTAL SECTION

**Materials and Methods.** All experiments with moisture- or air-sensitive compounds were performed in anhydrous solvents under nitrogen atmosphere in well-dried glassware. Dichloromethane, toluene, and *N*,*N*-dimethylmethanamide (DMF) were dried over calcium hydride and distilled prior to use. Pyridine was obtained from a commercial source and was used without further purification. THF was dried and distilled over sodium/benzophenone. Column chromatography was performed with silica gel (silica gel 60, Merck) or aluminum oxide (aluminum oxide 90, Merck). UV−vis−NIR absorption spectrum was measured with a JASCO V-570 spectrometer. For solid-state measurements, an ISN-723 integrating sphere was attached to a V-570 spectrometer. NMR spectra were obtained on Bruker Mercury300, JEOL GSX400, and JEOL GSX500 spectrometers. ESR and ENDOR spectra were recorded on a JEOL JES-SRE2X spectrometer equipped with a JEOL ES-EDX4 ENDOR spectrometer. For ENDOR measurements, $1 \times 10^{-3}$ M toluene solutions of **1a** and **1c** were prepared. The typical measurement conditions were 5 mW microwave power level and 0.1 mT modulation width (80 MHz). The RF power was set at 115 dB, and FM modulation frequency was 50 or 100 kHz. The spectrum was recorded at 202.9 K for **1a** and 163.2 K for **1c**. ESR spectral simulations were performed with Bruker SimFonia program. The small hyperfine coupling constants necessary for simulations were determined with the help of DFT calculation results. EI and MALDI-TOF mass spectra were taken by using a Shimadzu GC-2010 and Shimadzu AXIMA-CFR, respectively. The high-resolution mass spectra were analyzed by using Applied Biosystems Japan Ltd. Analyst QS 2.0 and ThermoXcalibur 2.1.0.1140 software. Data collections for X-ray crystal analysis were performed on a Rigaku/Varimax RAPID II diffractometer (Mo K$\alpha$, $\lambda$ = 0.71075 Å). The structures were solved with direct methods and refined with full-matrix least-squares (teXsan).[50] Cyclic voltammetry measurements were conducted with a BAS CV-50W electrochemical analyzer. The experiments employed a glassy carbon working electrode, a Pt counter electrode, and a $Ag/AgNO_3$ reference electrode in dichloromethane containing 0.1 M $Bu_4NClO_4$ as supporting electrolyte under a nitrogen atmosphere at room temperature.

**13*H*-Dibenzo[*a*,*i*]fluoren-13-one (3a).** To a solution of **6** (1.33 g, 5.0 mmol) in pyridine (80 mL) was added triton-B (40% in methanol, 5 mL), and the reaction mixture was stirred for 24 h at room temperature.[40,42] After the addition of concentrated HCl solution to pH < 4, the brown suspension was extracted with a large amount of dichloromethane, washed with brine, dried over $Na_2SO_4$, and filtered, and the solvent was removed in vacuo. Crude compound **3a** (1.40 g, quant.) was obtained as a brown powder.

**12*H*-Dibenzo[*b*,*h*]fluoren-12-one (3b).**[43] A mixture of **7** (4.22 g, 10 mmol), **9** (1.80 g, 10 mmol), and sodium iodide (9.74 g, 65.0 mmol) in DMF (80 mL) was heated to 80 °C for overnight. After cooling, the reaction was quenched by pouring into a 200 mL ice/water mixture and decolorized with sodium hydrogen sulfite. The resulting yellow precipitate (5.61 g, 88%) was collected as a crude product by filtration, dried under vacuum, and used in the next step without further purification.

**7*H*-Dibenzo[*c*,*g*]fluoren-7-one (3c).** A solution of **12** (3.42 g, 10 mmol) in acetic anhydride (35 mL) was heated to reflux for 1 h. Then the reaction mixture was concentrated under reduced pressure to obtain a brown residue, which was then heated to 300 °C for 3 h.[46] After cooling, dichloromethane was added to dissolve the remaining residue. **3c** (1.04 g, 37%) was collected as a red solid after being purified by silica gel column chromatography ($CH_2Cl_2$/*n*-hexane = 1:1, v/v).

**13-(9-Anthryl)-13*H*-dibenzo[*a*,*i*]fluoren-13-ol (2a).** To a solution of 9-bromoanthracene (514 mg, 2.0 mmol) in THF (30 mL) at −78 °C under nitrogen atmosphere was added dropwise *n*-BuLi (1.6 M in *n*-hexane, 1.25 mL, 2.0 mmol), and the reaction mixture was stirred at this temperature for 1 h. Then **3a** (280 mg, 1 mmol) was added, the reaction temperature was slowly raised to room temperature, and the mixture was stirred overnight. The reaction was quenched by saturated $NH_4Cl$ aqueous solution, extracted with diethyl ether, washed with brine, dried over $Na_2SO_4$, and then filtered. After column chromatography on silica gel ($CH_2Cl_2$/*n*-hexane = 1:4, v/v), **2a** (449 mg, 92%) was obtained as a yellow powder. Mp 115−116 °C. $R_f$ = 0.6 ($CH_2Cl_2$/*n*-hexane = 1:1, v/v); $^1$H NMR (500 MHz, $CDCl_3$) $\delta$ 10.41 (d, $J$ = 9.5 Hz, 2H), 8.41 (s, 1H), 8.09 (d, $J$ = 8.5 Hz, 1H), 8.02 (d, $J$ = 8.0 Hz, 2H), 7.92 (d, $J$ = 8.0 Hz, 2H), 7.73 (d, $J$ = 8.0 Hz, 2H), 7.66 (d, $J$ = 4.5 Hz, 2H), 7.64−7.65 (m, 2H), 7.55 (t, $J$ = 7.5 Hz, 1H), 7.49 (d, $J$ = 9.0 Hz, 1H), 7.42 (d, $J$ = 8.5 Hz, 2H), 7.14−7.18 (m, 2H), 6.90−6.94 (m, 3H), 6.55−6.85 (m, 1H) ppm; HRMS (ESI) $m/z$ $[M]^+$ calcd for $C_{35}H_{22}O$ 458.1665, found 458.1670.

**12-(9-Anthryl)-12*H*-dibenzo[*b*,*h*]fluoren-12-ol (2b).** The synthesis is very similar to that for **2a**. **2b** (92%) was also obtained as a yellow powder. Mp 133−134 °C. $R_f$ = 0. 5 ($CH_2Cl_2$/*n*-hexane = 1:1, v/v); $^1$H NMR (500 MHz, $CDCl_3$) $\delta$ 9.95 (d, $J$ = 9.0 Hz, 2H), 8.48 (s, 1H), 8.45 (s, 2H), 8.11 (d, $J$ = 7.5 Hz, 1H), 7.97 (d, $J$ = 8.5 Hz, 2H), 7.85 (d, $J$ = 8.0 Hz, 2H), 7.68 (s, 2H), 7.59−7.62 (m, 4H), 7.45−7.47 (m, 2H), 7.24−7.37 (m, 2H), 7.07 (t, $J$ = 6.5 Hz, 1H), 6.94 (d, $J$ = 9.5 Hz, 1H), 6.58−6.62 (m, 1H) ppm; HRMS (ESI) $m/z$ $[M]^+$ calcd for $C_{35}H_{22}O$ 458.1665, found 458.1666.

**7-(9-Anthryl)-7*H*-dibenzo[*c*,*g*]fluoren-7-ol (2c).** The synthesis is very similar to that for **2a**. **2c** (98%) was obtained also as a yellow powder. Mp 201−202 °C. $R_f$ = 0.3 ($CH_2Cl_2$/*n*-hexane = 1:1, v/v); $^1$H NMR (400 MHz, $CDCl_3$) $\delta$ 10.20 (d, $J$ = 8.8 Hz, 1H), 8.73 (d, $J$ = 8.4 Hz, 2H), 8.58 (s, 1H), 8.15 (d, $J$ = 7.6 Hz, 2H), 8.03 (d, $J$ = 8.0 Hz, 1H), 7.95 (d, $J$ = 7.6 Hz, 2H), 7.85 (d, $J$ = 8.4 Hz, 2H), 7.72 (t, $J$ = 7.8 Hz, 2H), 7.48−7.62 (m, 7H), 7.15 (t, $J$ = 7.4 Hz, 1H), 6.65 (t, $J$ = 7.8 Hz, 1H) ppm; HRMS (ESI) $m/z$ $[M - H]^+$ calcd for $C_{35}H_{21}O$ 457.1591, found 457.1587.

**13-(9-Anthryl)-13*H*-dibenzo[*a*,*i*]fluorene (2a′).** To a solution of **2a** (458 mg, 1 mmol) in dichloromethane (20 mL) at room temperature under nitrogen atmosphere were added dropwise


dx.doi.org/10.1021/ja507005c | J. Am. Chem. Soc. 2014, 136, 12784−12793

triethylsilane (0.2 mL) and trifluoroacetic acid (0.1 mL), and the reaction mixture was stirred at this temperature overnight. After distillation of the solvent and column chromatography on aluminum oxide ($CH_2Cl_2$/*n*-hexane = 1:50, v/v), **2a** (323 mg, 73%) was obtained as a gray powder. Mp 218−219 °C. $R_f$ = 0.4 ($CH_2Cl_2$/*n*-hexane = 1:5, v/v); $^1$H NMR (500 MHz, $CDCl_3$) $\delta$ 8.99 (d, $J$ = 9.0 Hz, 2H), 8.43 (s, 1H), 8.18 (d, $J$ = 8.5 Hz, 1H), 8.13 (d, $J$ = 8.5 Hz, 2H), 7.91 (d, $J$ = 8.0 Hz, 2H), 7.74 (m, 4H), 7.62 (t, $J$ = 6.5 Hz, 1H), 7.13 (m, 4H), 7.00 (m, 2H), 6.87 (d, $J$ = 9.0 Hz, 1H), 6.82 (t, $J$ = 7.0 Hz, 2H), 6.60 (t, $J$ = 8.0 Hz, 1H) ppm; HRMS (ESI) $m/z$ $[M]^+$ calcd for $C_{35}H_{22}$ 442.1716, found 442.1717.

**12-(9-Anthryl)-12*H*-dibenzo[*b,h*]fluorene (2b′).** The synthesis is very similar to that for **2a**′. **2b**′ (67%) was obtained also as a gray powder. Mp 150 °C (decomp). $R_f$ = 0.5 ($CH_2Cl_2$/*n*-hexane = 1:5, v/v); $^1$H NMR (400 MHz, $CDCl_3$) $\delta$ 8.76 (d, $J$ = 9.2 Hz, 1H), 8.56 (s, 2H), 8.52 (s, 1H), 8.18 (d, $J$ = 8.4 Hz, 1H), 8.02 (d, $J$ = 8.4 Hz, 2H), 7.91 (d, $J$ = 8.0 Hz, 1H), 7.68 (t, $J$ = 7.6 Hz, 1H), 7.60 (t, $J$ = 6.4 Hz, 1H), 7.54 (d, $J$ = 8.0 Hz, 2H), 7.45 (m, 4H), 7.34 (t, $J$ = 7.2 Hz, 2H), 7.14 (t, $J$ = 7.2 Hz, 1H), 6.95 (s, 1H), 6.82 (d, $J$ = 8.8 Hz, 1H), 6.69 (t, $J$ = 9.2 Hz, 1H) ppm; HRMS (ESI) $m/z$ $[M]^+$ calcd for $C_{35}H_{22}$ 442.1716, found 442.1720.

**7-(9-Anthryl)-7*H*-dibenzo[*c,g*]fluorene (2c′).** The synthesis is very similar to that for **2a**′. **2c**′ (66%) was obtained also as a gray powder. Mp 159−160 °C. $R_f$ = 0.5 ($CH_2Cl_2$/*n*-hexane = 1:5, v/v); $^1$H NMR (400 MHz, $CDCl_3$) $\delta$ 8.97 (d, $J$ = 8.8 Hz, 2H), 8.76 (d, $J$ = 8.8 Hz, 1H), 8.50 (s, 1H), 8.16 (d, $J$ = 8.4 Hz, 1H), 7.96 (d, $J$ = 8.4 Hz, 2H), 7.90 (d, $J$ = 8.0 Hz, 1H), 7.72 (d, $J$ = 8.0 Hz, 2H), 7.67 (m, 3H), 7.58 (m, 3H), 7.25 (m, 3H), 7.16 (t, $J$ = 7.2 Hz, 1H), 6.69 (m, 3H), 6.63 (s, 1H) ppm; HRMS (ESI) $m/z$ $[M]^+$ calcd for $C_{35}H_{22}$ 442.1716, found 442.1721.

**13-(9-Anthryl)-13*H*-dibenzo[*a,i*]fluorenyl Radical (1a).** A mixture of **2a** (229 mg, 0.5 mmol) and $SnCl_2$ (474 mg, 2.5 mmol) in dichloromethane (20 mL) was stirred at room temperature for 5 h under nitrogen atmosphere, and then the reaction mixture was filtered. After column chromatography on silica gel (*n*-hexane), **1a** was obtained as a black powder. Recrystallization of this powder in solution ($CH_2Cl_2$/toluene = 1:1, v/v) under argon flow gave a $\sigma$-dimer of **1a** (77 mg, 35%) as deep red needles. HRMS (ESI) $m/z$ $[M]^+$ calcd for $C_{35}H_{21}$ 441.1638, found 441.1644.

**12-(9-Anthryl)-12*H*-dibenzo[*b,h*]fluorenyl Radical (1b).** Oxidation method: An H-formed tube (Figure S13, SI) was used for generation and recrystallization of **2b**. A solution of **2′b** (88 mg, 0.2 mmol) in *n*-hexane (10 mL) was placed in A, and a solution of DDQ (23 mg, 0.1 mmol) in toluene (8 mL) in B. After the solutions were frozen, tube C was sealed. The solution was degassed by a repeated freeze−pump−thaw method (three times). Then the H-formed tube was sealed at D. The solution at B was transferred to A through the middle glass filter. After the mixed solution was heated at 50 °C for 2 h, the solution at A was transferred to B. Then tube A was submerged into water and slowly cooled by water evaporation naturally. After several weeks, the resulting brown crystals (34 mg, 38%) were collected by filtration in air after opening this sealed tube. Reduction method: A mixture of **2b** (229 mg, 0.5 mmol) and $SnCl_2$ (474 mg, 2.5 mmol) in dichloromethane (20 mL) was stirred at room temperature for 5 h under nitrogen atmosphere, and then the reaction mixture was filtered. After column chromatography on silica gel (*n*-hexane), **1b** was obtained as a black solid. Recrystallization of this powder in solution ($CH_2Cl_2$/toluene = 1:1, v/v) in the sealed H-formed tube gave **1b** (73 mg, 33%) as brown crystals. HRMS (ESI) $m/z$ $[M]^+$ calcd for $C_{35}H_{21}$ 441.1638, found 441.1645.

**7-(9-Anthryl)-7*H*-dibenzo[*c,g*]fluorenyl Radical (1c).** Oxidation method: The synthesis is very similar to that for **1b** and involved recrystallization in solution ($CH_2Cl_2$/ethyl acetate = 3:1, v/v) under argon flow to give the $\sigma$-dimer of **1c** (73%) as orange needles. Reduction method: The synthetic method is the same as that for **1a**. After column chromatography on silica gel (*n*-hexane), **1c** was obtained as a purple powder. Recrystallization of this powder in solution ($CH_2Cl_2$/ethyl acetate = 3:1, v/v) under argon flow gave a $\sigma$-dimer of **1c** (82%) as orange needles. The $\sigma$-dimer was dissolved in *n*-hexane and recrystallized at low temperature to give **1c** as purple crystals. HRMS (ESI) $m/z$ $[M]^+$ calcd for $C_{35}H_{21}$ 441.1638, found 441.1644.

**Computational Methods.** All DFT calculations were performed with the Gaussian 03 program.[51] The molecular geometries were optimized at the UB3LYP/6-31G** level of calculation. For the dimerization analysis, all optimized structures were checked by using harmonic frequency analysis as true minima with no imaginary frequencies or a transition state with only one imaginary frequency. Spin densities were estimated at the UBLYP/6-31G** level of calculation. TD calculations were performed at the UB3LYP/6-31G** level of calculation.

**Crystal Data for $\sigma$-Dimer of a-Type Radical ($1a_2$).** $C_{72}H_{46}Cl_4$, $M_r$ = 1052.89, monoclinic, space group $P2_1/c$, $a$ = 11.7320 (8) Å, $b$ = 17.4804 (11) Å, $c$ = 25.4536 (15) Å, $\beta$ = 96.9037 (14)°, $V$ = 5182.2 (6) Å$^3$, $Z$ = 4, $T$ = 200 K, $R1(wR2)$ = 0.066 (0.215) for 685 parameters and 11814 independent reflections, GOF = 1.01. CCDC 1012338.

**Crystal Data for b-Type Radical (1b).** $C_{35}H_{21}$, $M_r$ = 441.52, monoclinic, space group $P2_1/n$, $a$ = 12.9470 (4) Å, $b$ = 12.7291 (3) Å, $c$ = 28.2335 (6) Å, $\beta$ = 96.669 (1)°, $V$ = 4621.5 (2) Å$^3$, $Z$ = 8, $T$ = 200 K, $R1(wR2)$ = 0.051 (0.159) for 631 parameters and 10531 independent reflections, GOF = 1.16. CCDC 1012337.

**Crystal Data for c-Type Radical (1c).** $C_{35}H_{21}$, $M_r$ = 441.52, monoclinic, space group $C2/c$, $a$ = 14.719 (4) Å, $b$ = 13.335 (3) Å, $c$ = 13.137 (6) Å, $\beta$ = 118.001 (3)°, $V$ = 2276.6 (2) Å$^3$, $Z$ = 4, $T$ = 200 K, $R1(wR2)$ = 0.049 (0.127) for 160 parameters and 2603 independent reflections, GOF = 1.05. CCDC 1012336.

**Crystal Data for $\sigma$-Dimer of c-Type Radical ($1c_2$).** $C_{37}H_{23}Cl_6$, $M_r$ = 680.25, monoclinic, space group $P2_1/n$, $a$ = 9.5286 (9) Å, $b$ = 17.5723 (18) Å, $c$ = 19.0353 (17) Å, $\beta$ = 94.805 (14)°, $V$ = 3176.1 (5) Å$^3$, $Z$ = 4, $T$ = 200 K, $R1(wR2)$ = 0.083 (0.264) for 407 parameters and 7233 independent reflections, GOF = 0.89. CCDC 1012339.

## ■ ASSOCIATED CONTENT

### Ⓢ Supporting Information

ENDOR spectra (Figures S1 and S2). Time-dependent $^1$H NMR spectra of $\mathbf{1c}_2$ (Figure S3). Spin density map of anthracene-substituted fluorenyl radical (Figure S4). Energy diagram for twisted **1b** to $\mathbf{1b}_2$ (Figure S5). Time-dependent cyclic voltammograms of $\mathbf{1c}_2$ (Figure S6). Time-dependent UV−vis−NIR spectra of $\mathbf{1c}_2$ (Figure S7). Mechanochemical behavior in UV−vis−NIR spectra of **1a** and **1c** (Figure S8 and S9). Determination of half-life (Figure S10−S12). Molecular orbital diagrams. Details on the theoretical calculations. This material is available free of charge via the Internet at http://pubs.acs.org.

## ■ AUTHOR INFORMATION


### Corresponding Author

kubo@chem.sci.osaka-u.ac.jp

### Present Address

‡Department of Environmental and Biological Chemistry, Faculty of Engineering, Fukui University of Technology, Fukui City, Fukui 910-8507, Japan.


### Notes

The authors declare no competing financial interest.

## ■ ACKNOWLEDGMENTS

This work was supported in part by the Grants-in-Aid for Scientific Research on Innovative Areas "Organic Synthesis Based on Reaction Integration. Development of New Methods and Creation of New Substances" (No. 2105). Y.T. acknowledges the financial support from China Scholarship Council (CSC). The authors thank JASCO for the solid-state UV−vis−NIR measurements.

## REFERENCES


(1) Rajca, A. *Chem. Rev.* **1994**, *94*, 871.
(2) (a) Hicks, R. G. *Org. Biomol. Chem.* **2007**, *5*, 1321. (b) *Stable Radicals: Fundamental and Applied Aspects of Odd-electron Compounds*; Hicks, R., Ed.; Wiley-Blackwell: New York, 2010; pp 1−606.
(3) Rawson, J. M.; Alberola, A.; Whalley, A. *J. Mater. Chem.* **2006**, *16*, 2560.
(4) Raman, K. V.; Kamerbeek, A. M.; Mukherjee, A.; Atodiresei, N.; Sen, T. K.; Lazić, P.; Caciuc, V.; Michel, R.; Stalke, D.; Mandal, S. K.; Blügel, S.; Münzenberg, M.; Moodera, J. S. *Nature* **2013**, *493*, 509.
(5) Rocha, A. R.; García-Suárez, V. M.; Bailey, S. W.; Lambert, C. J.; Ferrer, J.; Sanvito, S. *Nat. Mater.* **2005**, *4*, 335.
(6) Suga, T.; Ohshiro, H.; Sugita, S.; Oyaizu, K.; Nishide, H. *Adv. Mater.* **2009**, *21*, 1627.
(7) Nishide, H.; Oyaizu, K. *Science* **2008**, *319*, 737.
(8) Morita, Y.; Nishida, S.; Murata, T.; Moriguchi, M.; Ueda, A.; Satoh, M.; Arifuku, K.; Sato, K.; Takui, T. *Nat. Mater.* **2011**, *10*, 947.
(9) Guasch, J.; Grisanti, L.; Souto, M.; Lloveras, V.; Vidal-Gancedo, J.; Ratera, I.; Painelli, A.; Rovira, C.; Veciana, J. *J. Am. Chem. Soc.* **2013**, *135*, 6958.
(10) Sugawara, T.; Matsushita, M. M. *J. Mater. Chem.* **2009**, *19*, 1738.
(11) Frantz, D. K.; Walish, J. J.; Swager, T. M. *Org. Lett.* **2013**, *15*, 4782.
(12) Matsuki, Y.; Maly, T.; Ouari, O.; Karoui, H.; Le Moigne, F.; Rizzato, E.; Lyubenova, S.; Herzfeld, J.; Prisner, T.; Tordo, P.; Griffin, R. G. *Angew. Chem., Int. Ed.* **2009**, *48*, 4996.
(13) Gabellieri, C.; Mugnaini, V.; Paniagua, J. C.; Roques, N.; Oliveros, M.; Feliz, M.; Veciana, J.; Pons, M. *Angew. Chem., Int. Ed.* **2010**, *49*, 3360.
(14) Mesa, J. A.; Velázquez-Palenzuela, A.; Brillas, E.; Coll, J.; Torres, J. L.; Juliá, L. *J. Org. Chem.* **2012**, *77*, 1081.
(15) Bobko, A. a; Dhimitruka, I.; Zweier, J. L.; Khramtsov, V. V. *J. Am. Chem. Soc.* **2007**, *129*, 7240.
(16) Sheldon, R. a.; Arends, I. W. C. E.; Ten Brink, G.-J.; Dijksman, A. *Acc. Chem. Res.* **2002**, *35*, 774.
(17) Aliaga, C.; Aspée, A.; Scaiano, J. C. *Org. Lett.* **2003**, *5*, 4145.
(18) Wright, J. S.; Johnson, E. R.; DiLabio, G. A. *J. Am. Chem. Soc.* **2001**, *123*, 1173.
(19) (a) Simão, C.; Mas-Torrent, M.; Crivillers, N.; Lloveras, V.; Artés, J. M.; Gorostiza, P.; Veciana, J.; Rovira, C. *Nat. Chem.* **2011**, *3*, 356. (b) Mas-Torrent, M.; Crivillers, N.; Rovira, C.; Veciana, J. *Chem. Rev.* **2011**, *112*, 2506.
(20) Kawanaka, Y.; Shimizu, A.; Shinada, T.; Tanaka, R.; Teki, Y. *Angew. Chem., Int. Ed.* **2013**, *52*, 6643.
(21) Gryn'ova, G.; Marshall, D. L.; Blanksby, S. J.; Coote, M. L. *Nat. Chem.* **2013**, *5*, 474.
(22) *Magnetic Properties of Organic Materials*; Lathi, P. M., Ed.; Marcel Dekker: New York, 1999; pp 1−728.
(23) Griller, D.; Ingold, K. U. *Acc. Chem. Res.* **1976**, *9*, 13.
(24) Kitagawa, T.; Ogawa, K.; Komatsu, K. *J. Am. Chem. Soc.* **2004**, *126*, 9930.
(25) Janiak, C.; Weimann, R.; Görlitz, F. *Organometallics* **1997**, *16*, 4933.
(26) Sitzmann, H.; Boese, R. *Angew. Chem., Int. Ed. Engl.* **1991**, *30*, 971.
(27) Chase, D. T.; Rose, B. D.; McClintock, S. P.; Zakharov, L. N.; Haley, M. M. *Angew. Chem., Int. Ed.* **2011**, *50*, 1127.
(28) Chase, D. T.; Fix, A. G.; Rose, B. D.; Weber, C. D.; Nobusue, S.; Stockwell, C. E.; Zakharov, L. N.; Lonergan, M. C.; Haley, M. M. *Angew. Chem., Int. Ed.* **2011**, *50*, 11103.
(29) Fix, A. G.; Deal, P. E.; Vonnegut, C. L.; Rose, B. D.; Zakharov, L. N.; Haley, M. M. *Org. Lett.* **2013**, *15*, 1362.
(30) Shimizu, A.; Tobe, Y. *Angew. Chem., Int. Ed.* **2011**, *50*, 6906.
(31) Shimizu, A.; Kishi, R.; Nakano, M.; Shiomi, D.; Sato, K.; Takui, T.; Hisaki, I.; Miyata, M.; Tobe, Y. *Angew. Chem., Int. Ed.* **2013**, *52*, 6076.
(32) Wang, J.; Wan, W.; Jiang, H.; Gao, Y.; Jiang, X.; Lin, H.; Zhao, W.; Hao, J. *Org. Lett.* **2010**, *12*, 3874.
(33) Lee, C.-H.; Lai, Y.-Y.; Cheng, S.-W.; Cheng, Y.-J. *Org. Lett.* **2014**, *16*, 936.
(34) Dalton, D. R.; Siebman, S. A. *J. Am. Chem. Soc.* **1969**, *91*, 1194.
(35) Gostowski, R. C.; Sabrinia, T. B.; Bonner, S. D.; Emrich, E. E.; Steelman, S. L. *J. Phys. Org. Chem.* **2000**, *13*, 735.
(36) Font-Sanchis, E.; Aliaga, C.; Bejan, E. V.; Cornejo, R.; Scaiano, J. C. *J. Org. Chem.* **2003**, *68*, 3199.
(37) Simonet, J.; Jouikov, V. *Electrochem. Commun.* **2011**, *13*, 254.
(38) Azuma, N.; Ozawa, T.; Yamauchi, J. *Bull. Chem. Soc. Jpn.* **1994**, *67*, 31.
(39) Koelsch, C. F. *J. Am. Chem. Soc.* **1957**, *79*, 4439.
(40) Kubo, T.; Katada, Y.; Shimizu, A.; Hirao, Y.; Sato, K.; Takui, T.; Uruichi, M.; Yakushi, K.; Haddon, R. C. *J. Am. Chem. Soc.* **2011**, *133*, 14240.
(41) (a) Zeng, Z.; Sung, Y. M.; Bao, N.; Tan, D.; Lee, R.; Zafra, J. L.; Lee, B. S.; Ishida, M.; Ding, J.; López Navarrete, J. T.; Li, Y.; Zeng, W.; Kim, D.; Huang, K.-W.; Webster, R. D.; Casado, J.; Wu, J. *J. Am. Chem. Soc.* **2012**, *134*, 14513. (b) For a recent review on singlet biradicals, see Sun, Z.; Zeng, Z.; Wu, J. *Acc. Chem. Res.* **2014**, DOI: 10.1021/ar5001692.
(42) Rabinovitz, M.; Agranat, I.; Weitzen-Dagan, A. *Tetrahedron Lett.* **1974**, *15*, 1241.
(43) Morris, J. L.; Becker, C. L.; Fronczek, F. R.; Daly, W. H.; McLaughlin, M. L. *J. Org. Chem.* **1994**, *59*, 6484.
(44) Becker, C. L.; McLaughlin, M. L. *Synlett* **1991**, *1991*, 642.
(45) Colletti, S. L.; Halterman, R. L. *Organometallics* **1991**, *10*, 3438.
(46) Nishiura, C.; Kamatani, J.; Abe, S. US Patent, 8,431,249 B2, 2013.
(47) **1c** possesses a spin density at the 10-position of the anthryl group larger than that of **1b**. This might arise from small differences in the twist angle between dibenzofluorenyl and anthryl (68° for **1b** and 66° for **1c**) and spin density on connected carbon atoms in the Cp rings (+0.496 for **1b**′ and +0.504 for **1c**′, see Figure 5).
(48) Chen, Z.; Wannere, C. S.; Corminboeuf, C.; Puchta, R.; Schleyer, P. v. R. *Chem. Rev.* **2005**, *105*, 3842.
(49) Biedermann, P. U.; Stezowski, J. J.; Agranat, I. *Eur. J. Org. Chem.* **2001**, *2001*, 15.
(50) Kaupp, G. *CrystEngComm* **2009**, *11*, 388.
(51) Frisch, M. J.; Trucks, G. W.; Schlegel, H. B.; Scuseria, G. E.; Robb, M. A.; Cheeseman, J. R.; Montgomery, Jr., J. A.; Vreven, T.; Kudin, K. N.; Burant, J. C.; Millam, J. M.; Iyengar, S. S.; Tomasi, J.; Barone, V.; Mennucci, B.; Cossi, M.; Scalmani, G.; Rega, N.; Petersson, G. A.; Nakatsuji, H.; Hada, M.; Ehara, M.; Toyota, K.; Fukuda, R.; Hasegawa, J.; Ishida, M.; Nakajima, T.; Honda, Y.; Kitao, O.; Nakai, H.; Klene, M.; Li, X.; Knox, J. E.; Hratchian, H. P.; Cross, J. B.; Bakken, V.; Adamo, C.; Jaramillo, J.; Gomperts, R.; Stratmann, R. E.; Yazyev, O.; Austin, A. J.; Cammi, R.; Pomelli, C.; Ochterski, J. W.; Ayala, P. Y.; Morokuma, K.; Voth, G. A.; Salvador, P.; Dannenberg, J. J.; Zakrzewski, V. G.; Dapprich, S.; Daniels, A. D.; Strain, M. C.; Farkas, O.; Malick, D. K.; Rabuck, A. D.; Raghavachari, K.; Foresman, J. B.; Ortiz, J. V.; Cui, Q.; Baboul, A. G.; Clifford, S.; Cioslowski, J.; Stefanov, B. B.; Liu, G.; Liashenko, A.; Piskorz, P.; Komaromi, I.; Martin, R. L.; Fox, D. J.; Keith, T.; Al-Laham, M. A.; Peng, C. Y.; Nanayakkara, A.; Challacombe, M.; Gill, P. M. W.; Johnson, B.; Chen, W.; Wong, M. W.; Gonzalez, C.; Pople, J. A. *Gaussian 03, revision D.01*; Gaussian, Inc., Wallingford, CT, 2004.